IEEE Access
Multidisciplinary | Rapid Review | Open Access Journal

Received November 6, 2019, accepted January 1, 2020, date of publication January 13, 2020, date of current version January 21, 2020.

Digital Object Identifier 10.1109/ACCESS.2020.2966005

Wake Features of Moving Submerged Bodies and Motion State Inversion of Submarines

FUDUO XUE, WEIQI JIN, SU QIU, AND JIE YANG
MOE Key Laboratory of Optoelectronic Imaging Technology and System, Beijing Institute of Technology, Beijing 100081, China
Corresponding author: Weiqi Jin (jinwq@bit.edu.cn)

This work was supported by the NSFC under Project 61575023.

ABSTRACT The interaction between a moving submerged body and a homogeneous/stratified fluid generates a Bernoulli hump, a Kelvin wake, and an internal wake on the water surface. The height distribution of wakes is directly related to the location and motion state of the submerged body. Thus, it is possible to retrieve kinematics information of a submarine from the images of wakes obtained by photoelectric detection equipment. In order to extract the submarine's location and velocity information effectively from the wake photoelectric images, we investigate the relationship between the motion state of moving submerged bodies and wakes in this paper. Bernoulli hump, Kelvin wake, and internal wake models are established based on potential flow theory and thin-ship approximation. We analyzed the wave crestline pattern and the energy characteristics of Kelvin wake components (divergent and transverse waves) and internal wakes at different velocities and diving depths. Finally, we propose a method for estimating the velocity of a submarine based on the wake wavelength and the diving depth inversion method based on the Fourier power spectrum of the Kelvin wake. The results obtained prove the feasibility of using photoelectric equipment to obtain wake images for use in analyzing the kinematics state of submarines, which are of guiding significance for detection and information processing in real-scale submarines.

INDEX TERMS Bernoulli hump, Fourier spectrum, internal wake, Kelvin wake, moving submerged body.

I. INTRODUCTION

Underwater target detection is a key technology for marine defense that focuses on antisubmarine warfare. Timely and accurate detection of underwater targets and determination of their location, diving depth, speed, and other information are vital in antisubmarine technologies. With the development of sound absorption technology, the traditional method of using sonar to directly detect undersea submarines has become increasingly difficult. Therefore, nonacoustic detection methods are imperative. As LIDAR images are severely distorted by sea waves, the indirect detection of undersea targets via sea surface wakes generated by moving submerged bodies has become a trend in nonacoustic detection technologies. Currently, wake detection is achieved through photoelectric imaging equipment such as synthetic aperture radar (SAR) [1]–[5] and infrared thermal radiation detectors [6]–[8]. There are also reports on the magnetic detection of wakes using electromagnetic perturbation induced by the motion of conductive seawater [9], [10].

In marine environments, the interaction between a moving submerged body and surrounding fluid can generate four kinds of wakes: Bernoulli hump, Kelvin wake, internal wake, and turbulent wake. The Bernoulli hump is a surface wave unique to underwater objects moving near the water surface [11]. It is located directly above the submerged body and can be regarded as a near-field component of the Kelvin wake system. The Kelvin wake is one of the most thoroughly studied surface waves because of its regular structure [1], [2]. It is generated in homogeneous fluids. Its far-field region contains two distinct waveforms: divergent and transverse waves (see Figure 1). Divergent waves diffuse to both sides of a submerged body, whereas transverse waves propagate to the rear of the submerged body. Previous studies have shown that the wave height distribution of a Kelvin wake is directly related to the motion state of an underwater object [1], [4]. Several recent studies also suggest that the Kelvin wake can produce a larger wake angle than the classical value(19.5°) in the presence of vorticities or with a large Froude

The associate editor coordinating the review of this manuscript and approving it for publication was Geng-Ming Jiang.

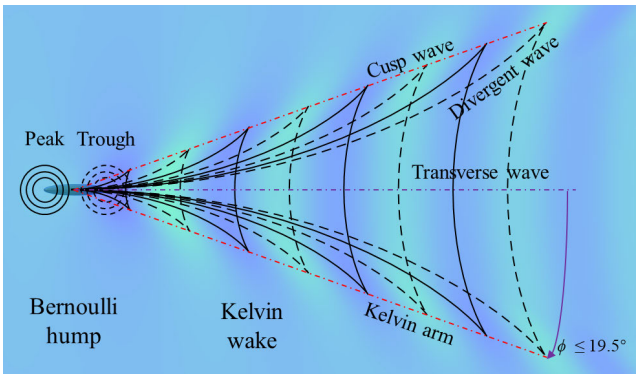

FIGURE 1. Bernoulli hump and Kelvin wake induced by a submarine. The Bernoulli hump is directly above the submarine, while the Kelvin wake is at the rear. The Kelvin wake is a superposition of divergent and transverse waves, with cusp waves and Kelvin arms on the outer edges. In classical theory, the angle between the Kelvin arm and the central axis is 19.5°. In practice, when the diving depth is shallow, as the velocity increases (Froude number increases), the wake angle is usually less than this value.

number (greater than 1) [12], [13]. At the same time, when the submarine is moving near the water surface, the Kelvin wake angle may decrease with the increase of Froude number (less than 1), this is considered to be caused by the constructive interference of the positive bow waves and negative stern waves [14]. The internal wake is generated by disturbance in a stratified fluid [10]. Because a pycnocline exists in oceans all year round, it is more likely to generate internal wakes when submerged bodies move in deep water. A turbulent wake is the trail formed by bubble foam generated by submarine propellers floating up to the water surface [8]. It is basically invisible when the diving depth is deep. In summary, to comprehensively study the relationship between wakes and the motion state of a moving submerged body, reliable simulation of the Kelvin wake (including the Bernoulli hump) and the internal wake is required.

Retrieving the ship motion state using features of a wake is an important application of the study of wake characteristics. The interaction between the surface current of a Kelvin wake or an internal wake with the capillary gravity wave modulates the roughness of the sea surface, so that the wake can be imaged optically or by SAR [2]. Using Radon transform coupled with wavelet [15], sparse representation [16] or artificial neural network [17] to obtain linear features in the image, some important wake features such as wavelength and wake angle can be obtained. In recent years, significant progress has been made in using these wake features to retrieve the moving speed of surface vessels [1], [18]. Several algorithms have also been proposed to improve the inversion accuracy [19]. It can be proved that these algorithms can also be used to estimate the velocity of submarines through analysis. There is little discussion on the relationship between wake characteristics and the diving depth of submerged bodies. In this paper, we propose a simple method for inversing the diving depth of a submerged body based on the Kelvin wake Fourier power spectrum. In addition, we discuss the influence of the shape of the submerged body and environmental factors on inversion accuracy.

The remainder of this paper is organized as follows. Section II describes the modeling of the Kelvin wake and the internal wake induced by a moving submerged Rankine ellipsoid. Section III details the relationship between the motion state of a submerged body and its wake characteristics. Section IV presents the proposed motion state inversion method and discusses the results obtained from simulations. Finally, Section V serves as a conclusion for the paper.

II. MODELING OF WAKES INDUCED BY SUBMARINES

A. KELVIN WAKE

To accurately and reliably model a Kelvin wake, we used the potential flow theory for our simulation. Consider the case shown in Figure 2. It is assumed that a submarine is moving below the water surface at a velocity U. It is considered that the flow field is infinitely deep and the fluid is incompressible. Turbulence generated by the propeller is not considered. A right-hand Cartesian coordinate system is constructed. The x axis points in the opposite direction of the motion of the submerged body. The z axis points to the bottom of the flow field, and the z coordinate at the water surface is zero. To better reflect the shape of modern submarines, the submerged body is considered to be a slender Rankine ellipsoid with half-length l and half-width b, with a length to beam ratio, l/b, of 10:1 (in this paper, $l = 50$ m, $b = 5$ m). The distance from the long axis of the ellipsoid to the water surface (i.e., the diving depth) is h_0.

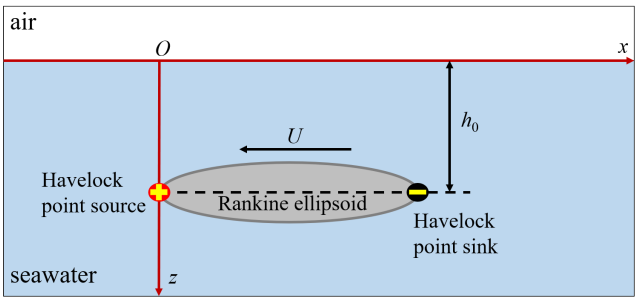

FIGURE 2. Moving submerged Rankine ellipsoid of velocity U and diving depth h_0 in an infinite depth homogeneous fluid of density ρ.

For incompressible fluids, the wake velocity field, $\mathbf{v}$, can be expressed according to the potential flow theory by its potential function, ϕ: $\mathbf{v} = -\nabla\phi$. The velocity potential satisfies the following Laplace equations and boundary conditions [20]:

$$\nabla^2\phi = 0 \quad \text{in the flow field} \tag{1}$$

$$\frac{\partial\phi}{\partial n} = 0 \quad \text{on a free surface} \tag{2}$$

$$\frac{\partial\phi}{\partial n} = 0 \quad \text{on the submerged body surface} \tag{3}$$

$$p = \frac{1}{2}\rho(U^2 - \phi_x^2 - \phi_y^2 - \phi_z^2) = 0 \quad \text{on a free surface} \tag{4}$$

where n represents the normal vector. p is the excess pressure, representing the pressure above the atmospheric on the free

water surface, which is determined by the Bernoulli equation, namely equation (4). Newman [21] solved the problem of lack of an analytical solution to the above equations by linearizing the kinematics and dynamics equations on the free water surface, whereas Scullen and Tuck [22] solved the wave height of a Kelvin wake induced by a slender underwater body using the thin-ship approximation. This paper references their research to conduct thin-ship approximation: A Kelvin wake induced by a Rankine ellipsoid with a high length to beam ratio is equivalent to the wake induced by a pair of Havelock point sources/sinks, $\pm G$, distributed at the head and tail of the ellipsoid. The strength of the point source/sink is $2\pi Ub^2/3$. The velocity potential can be approximately expressed as [9]

$$\phi(x, y, z) = \frac{2\pi Ub^2}{3}\left[G(x, y, z) - G(x - 2l, y, z)\right] \quad (5)$$

Assuming that the viscosity of the fluid, γ, is equal to 0, the closed expression for G can be obtained by solving the velocity potential satisfying (1)–(4) in polar coordinates. G is a Green's function consisting of four parts:

$$G = G_1 + G_2 + G_3 + G_4 \quad (6)$$

$$G_1 = \frac{1}{4\pi R_1}, \quad R_1 = \sqrt{x^2 + y^2 + (z - h_0)^2} \quad (7)$$

$$G_2 = \frac{1}{4\pi R_2}, \quad R_2 = \sqrt{x^2 + y^2 + (z + h_0)^2} \quad (8)$$

$$G_3 = \frac{1}{\pi}\mathrm{Im}\int_{-\pi/2}^{\pi/2} u(\Omega)k_p \exp[-k(z + h_0) + jk_p\Omega]d\theta$$

$$k_p = k_0 \sec^2\theta, \quad \Omega(x, y, \theta) = x\cos\theta + y\sin\theta \quad (9)$$

$$u(\Omega) = \begin{cases} 1 & \Omega > 0 \\ 0 & \Omega \le 0 \end{cases}$$

$$G_4 = \frac{1}{(2\pi)^2}\mathrm{Re}\int_{-\pi/2}^{\pi/2} \Theta(x, y, z, \theta)d\theta$$

$$\Theta = \int_0^{+\infty} k\left\{\frac{2k_p}{k - k_p}\exp[-k(z + h_0) + jk\Omega]\right\}_{k=(1\pm j)d\eta} \quad (10)$$

where $k_0 = g/U^2$ (i.e., the cutoff wavenumber mentioned below) and g is the acceleration due to gravity, which is taken to be 9.81 m/s^2. The G_1 and G_2 terms constitute the velocity potential of the Bernoulli hump; the G_3 term corresponds to the far-field Kelvin wake; and the G_4 term is negligible compared with the first three terms. The wake velocity potential ϕ is solved using (1)–(7), and the wave height distribution of the Kelvin wake is finally obtained by the partial derivation of ϕ:

$$\zeta(x, y) = \frac{U}{g}\frac{\partial\phi}{\partial x}\bigg|_{z=0} \quad (11)$$

We numerically calculated the equations (5)–(11) to simulate the Kelvin wakes excited by submerged Rankine bodies with different sizes, speeds, and depths based on the potential flow theory and the thin-ship approximation, using the MATLAB (version 2019a) platform. The simulation results are independent from the grid resolution. A typical wake wave height distribution is shown in Figure 3. It can be clearly seen that the Bernoulli hump distributes directly above the location of the submerged body, whereas the Kelvin divergent and transverse wave components distribute on the water surface behind the submerged body. Using this method, the simulation time for each case on a PC with 2.7 GHz CPU and 16 GB memory is less than 2 min. Compared with our previous work on solving the Reynolds-Averaged Navier-Stokes (RANS) equation using computational fluid dynamics (CFD) software, ANSYS Fluent [23], the potential flow method has comparable simulation accuracy (with the same resolution) on the whole wave field (based on RMS error of the whole wave field according to [24]), but requires much less calculation time.

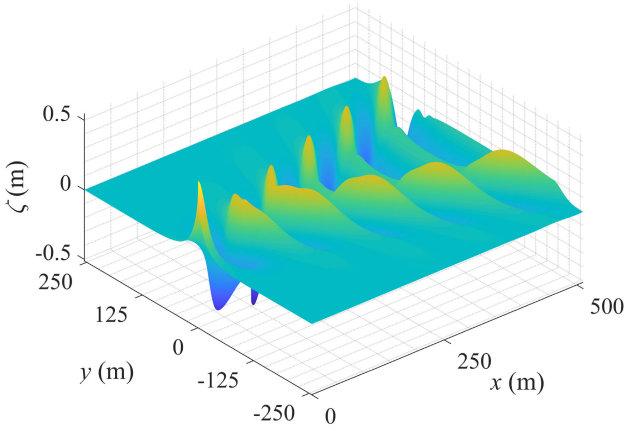

FIGURE 3. Kelvin wake pattern simulated by the potential flow method for submerged body of $U = 10$ m/s and $h_0 = 15$ m moving in the homogeneous fluid.

B. INTERNAL WAKE

Internal wakes are generated by disturbances in density in inhomogeneous fluids. Fluids with step changes in density (stratified fluids) are relatively simple cases. We simulated the internal wake induced by a Rankine submerged body in a two-layer fluid of finite depth. Consider the case of a submerged body moving in the upper fluid (see Figure 4).

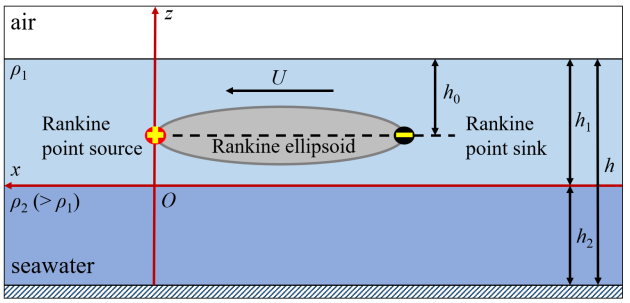

FIGURE 4. Moving submerged Rankine ellipsoid of velocity U and diving depth h_0 in a finite depth two-layer fluid of densities ρ_1 and ρ_2.

The depth of the flow field is h, and the upper and lower fluid depths are h_1 and h_2, respectively; the densities are ρ_1 and ρ_2 ($\rho_2 > \rho_1$, and $\rho_1 = 998.2$ kg/m^3, $\rho_2 = 1024$ kg/m^3). The distance from the long axis of the ellipsoid to the water surface is h_0. Similar to the discussion of the Kelvin wake, the submerged body is approximated as a pair of point sources/sinks distributed at the head and tail of a Rankine ellipsoid, and the Cartesian coordinate system is constructed with the interface as the xOy plane. The point source velocity potential, ϕ, satisfies the following governing equations and boundary conditions [25]:

$$\begin{aligned} \nabla^2\phi^{(1)} &= \delta(x, y, z-h_0), \quad \nabla^2\phi^{(2)} = 0 \\ k_0\phi_z^{(1)} + \phi_{xx}^{(1)} - \mu\phi_x^{(1)} &= 0, \quad z = h_1 \qquad (12) \\ \gamma(k_0\phi_z^{(1)} + \phi_{xx}^{(1)} - \mu\phi_x^{(1)}) &= k_0\phi_z^{(2)} + \phi_{xx}^{(2)} - \mu\phi_x^{(2)}, \quad z = 0 \qquad (13) \\ \phi_z^{(1)} &= \phi_z^{(2)}, \quad z = 0 \\ \phi_z^{(2)} &= 0, \quad z = -h_2 \\ \lim_{x\to+\infty} \nabla\phi^{(m)} &= 0 \qquad (14) \end{aligned}$$

where k_0 is as defined above, $\gamma = \rho_1/\rho_2$, $\varepsilon = 1-\gamma$, and μ is a proportionality constant that will be taken as zero later. The superscript $m = 1, 2$ refers to the free surface and interface, respectively. We constructed a cylindrical coordinate system (r, ψ, z). Using the potential flow method and the thin-ship approximation to solve the Green's function corresponding to the velocity potential, the far-field wave height of the internal wake at the free surface and the fluid interface is obtained as

$$\begin{aligned} \zeta(m) &\sim \sum_{n=1}^{2} \mathrm{Re}\left\{\int_{-\frac{\pi}{2}}^{\frac{\pi}{2}-\psi} P^{(m)}(k_n, \theta) e^{j(\frac{r}{h}) f_n(\theta,\psi)} d\theta\right\} \\ & r/h \gg 1 \qquad (15) \\ f_n(\theta, \psi) &= -hk_n \cos(\theta + \psi) \\ k_n &= \frac{1}{2} k_0 \sec^2\theta \Omega_n(k_n) \\ \Omega_n(k) &= \frac{t_1 + t_2}{1 + \gamma t_1 t_2} \\ &\quad \times \left[1 + (-1)^{n+1} \sqrt{1 - 4(1-\gamma)\frac{t_1 t_2 (1+\gamma t_1 t_2)}{(t_1+t_2)^2}}\right] \\ t_n &= \tanh kh_n, \quad n = 1, 2 \qquad (16) \end{aligned}$$

where $n = 1, 2$ denotes the surface-wave mode and the internal-wave mode, respectively:

$$\begin{aligned} f_n(\theta, \psi) &= -hk_n \cos(\theta + \psi) \\ P^{(1)} &= [Uk_n \cos\theta H^{(1)}/(g\Delta')]\Big|_{z=h1} \\ P^{(2)} &= [Uk_n \cos\theta (H^{(2)} - \gamma H^{(1)})/(\varepsilon g\Delta')]\Big|_{z=0} \qquad (17) \\ H^{(1)}(k_n, \theta) &= -8k_n k_0 \sec^2\theta \cdot \{\varepsilon \cosh[k_n(h - z - (h_1 - h_0))] \\ &\quad + \gamma \cosh[k_n(d - z - (h_1 - h_0))]\} \\ &\quad + 4\varepsilon(k_n^2 + k_0^2 \sec 4\theta) \sinh[k(h - z - (h_1 - h_0))] \\ &\quad + 4[(1+\gamma)k_n^2 - \varepsilon k_0^2 \sec^4\theta] \sinh[k((h_1 - h_2) - z \\ &\quad - (h_1 - h_0))] - 4\{[(1+\gamma)k_n^2 + 2k_n k_0 \sec^2\theta \\ &\quad + \varepsilon k_0^2 \sec^4\theta] \exp(-k_n h) + \varepsilon(k_n^2 - k_0^2 \sec^4\theta) \\ &\quad \cdot \exp(-k_n(h_1 - h_2))\} \cosh[k_n(z - (h_1 - h_0))] \end{aligned}$$

$$\begin{aligned} H^{(2)}(k_n, \theta) &= 16\gamma \cosh[k_n(h2 + z)]\{k_n^2 \sinh[k_n(h_1 - (h_1 - h_0))] \\ &\quad - k_n k_0 \sec 2\theta \cosh[k_n(h_1 - (h_1 - h_0))]\} \\ \Delta'(k_n, \theta) &= 4k_n[(1+\gamma) - hk_0 \sec^2\theta] \cosh k_n h \\ &\quad + 2[(1+\gamma)hk_n^2 - 2k_0 \sec^2\theta + \varepsilon h k_0^2 \sec^4\theta] \\ &\quad \times \sin kh + 4\varepsilon k \cosh k(h_1 - h_2) \\ &\quad + 2\varepsilon(h_1 - h_2)(k_n^2 - k_0^2 \sec^4\theta) \sin k(h_1 - h_2) \qquad (18) \end{aligned}$$

The wave height induced by a point sink can be obtained by moving the point source coordinates to $(-2l, 0, h_1 - h_0)$ and repeating the above analysis. The wave height distribution of the internal wake generated by a submerged Rankine body can ultimately be obtained by subtraction of the wave heights induced by a point source and a point sink. When the submerged body moves in the lower fluid, the governing equations and boundary conditions are exactly the same as those in the upper fluid, except that $h_0 > h_1$. The calculation of the internal wake wave height for a point source in the lower fluid is not described in this paper. Further details on how the internal wake wave height is derived can be found in [26]. We numerically calculated the equations (15)–(18) to simulate a typical distribution of an internal wake on a water surface in MATLAB, as shown in Figure 5. The simulation result is also independent from the grid resolution. The simulation of the internal wake using potential flow theory is also achieved in a short duration (i.e., the same operating conditions as the Kelvin wake simulation, 3–5 min).

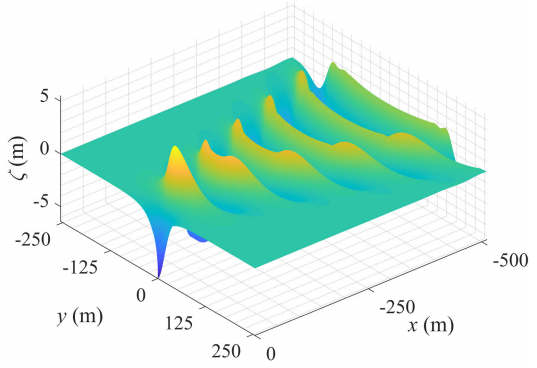

FIGURE 5. Internal wake pattern simulated by the potential flow method for submerged body of $U = 12$ m/s and $h_0 = 20$ m moving in the upper layer of the stratified fluid.

III. ANALYSIS OF SUBMARINE-GENERATED WAKE CHARACTERISTICS

A. WAVE HEIGHT DISTRIBUTION CHARACTERISTICS OF THE KELVIN WAKE IN THE FAR FIELD

1) SAME DIVING DEPTH, DIFFERENT VELOCITIES

The polar coordinate expression for Kelvin's divergent and transverse wave structures is as follows [1], [2]:

$$k_{1,2}(\theta, n) = \frac{4\pi U^2(8n - \varepsilon_{1,2})}{g(3 \mp \sqrt{1 - 8\tan^2\theta})^{\frac{3}{2}}} \cdot \frac{\sin\theta}{(1 \pm \sqrt{1 - 8\tan^2\theta})^{\frac{1}{2}} \cos^2\theta} \qquad (19)$$

where $\varepsilon_1 = 1$, $\varepsilon_2 = 3$, corresponding to the divergent wave and the transverse wave components, respectively, n is the number of periods, and θ is the angle between the normal vector of the Kelvin wake wave front and the direction of motion of the submerged body. For transverse waves, $0° \leq \theta \leq 35°16'$, whereas for divergent waves, $35°16' \leq \theta \leq 90°$. The crest/trough structure of a far-field Kelvin wake can be drawn using (10) (see Figure 6), and the wavelengths of the transverse and divergent waves can be obtained as follows:

$$\lambda = \lambda_{transverse} = \frac{2\pi U^2}{g} \tag{20}$$

$$\lambda_{divergent} = \frac{2\pi U^2}{g} \cos^2\theta \tag{21}$$

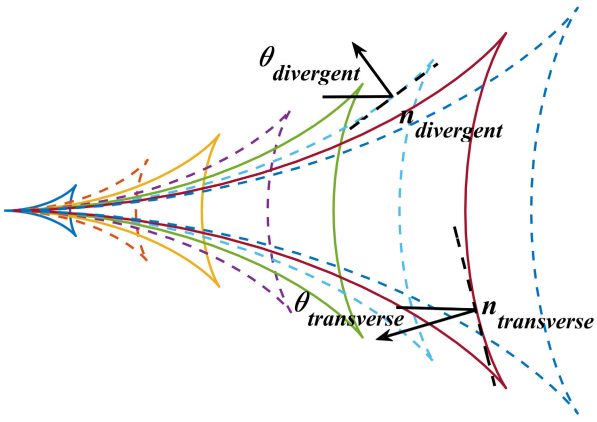

FIGURE 6. Illustration of structures of the Kelvin's divergent and transverse waves. The crests are solid lines and the troughs are dotted lines. θ is the angle between the normal vector (n of the wave front and the direction of motion of the submerged body.

The effect of velocity on the wave height distribution of the Kelvin wake is mainly reflected by the Froude number defined by the length of submerged body:

$$Fr_L = \frac{U}{\sqrt{gL}} = \frac{U}{\sqrt{2gl}} \tag{22}$$

We simulated the Kelvin wakes of the submerged body at the same diving depth ($h_0 = 15$ m) at different velocities (see Figure 7). The results show that as the velocity increases, the Froude number increases, the maximum wave height of the near-field Kelvin wake increases monotonically, while the far-field Kelvin wake has an oscillating wave height; the correctness of (19)–(21) can be verified by measuring structural parameters such as wavelength (λ) and angle (θ).

2) SAME VELOCITY, DIFFERENT DIVING DEPTHS

We simulated the Kelvin wakes of the submerged body at the same velocity ($U = 15$ m/s) and different diving depths (see Figure 8). It was observed that increasing the diving depth does not significantly affect the position of the Kelvin wake structure, which is consistent with (19). Visually, the Kelvin wake transforms from the divergent wave mode to the transverse wave mode. According to [4] and [27], the far-field

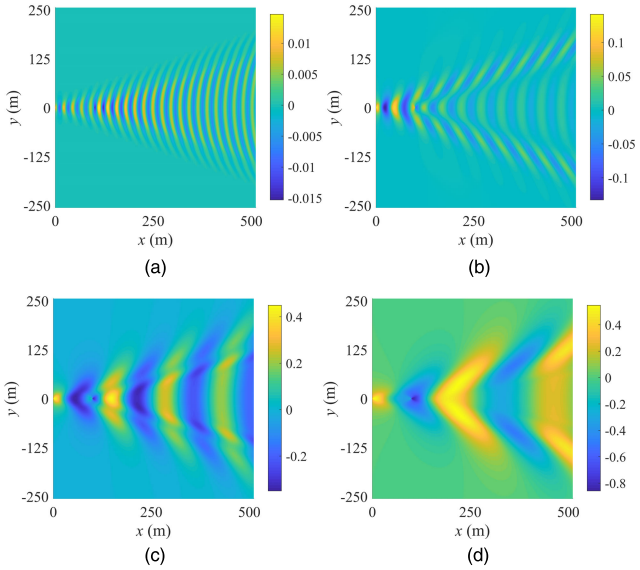

FIGURE 7. Kelvin wake patterns at four velocities (Froude numbers) and the same diving depth, $h_0 = 20$ m. (a) $U = 6$ m/s ($Fr_L = 0.19$), (b) $U = 9$ m/s ($Fr_L = 0.29$), (c) $U = 15$ m/s ($Fr_L = 0.48$), and (d) $U = 20$ m/s ($Fr_L = 0.64$).

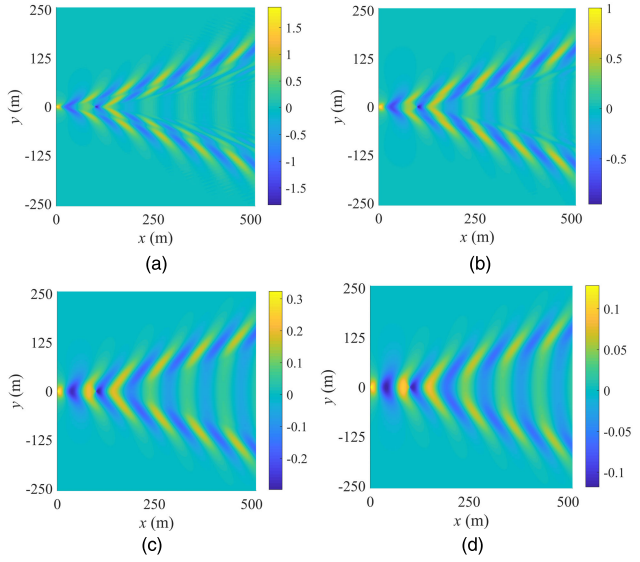

FIGURE 8. Kelvin wake patterns at four diving depths and the same velocity, $U = 12$ m/s ($Fr_L = 0.38$). (a) $h_0 = 6$ m, (b) $h_0 = 10$ m, (c) $h_0 = 20$ m, and (d) $h_0 = 30$ m.

Kelvin wake expression for an underwater dual-point source is equivalent to the far-field wake formula of a single-point source at the water surface; the latter is the former multiplied by an exponential attenuation term associated with $\sec^2\theta$. Consider the geometric meaning of θ, which refers to the angle between the transverse/divergent wave front vector and the direction of motion of the point source. The closer this is to the central axis, the smaller the value of θ for transverse waves ($\sec^2\theta \to 1$) and the larger the θ for divergent waves ($\sec^2\theta \to 0$). Both the transverse and divergent waves on the wake's outermost Kelvin arm have the same attenuation speed for a given diving depth; close to the central axis,

transverse waves have lower attenuation whereas divergent waves have higher attenuation, eventually leading to the phenomenon of the wake divergent/transverse mode transition, as shown in Figure 8.

3) KELVIN WAKE ANGLE BEHAVIOR

We also analyzed the Kelvin wake angle behavior with respect to velocity (Froude number) and diving depth. Here, the wake angle is defined as the angle between the line connecting the locations of the points associated with the highest peaks inside the wake and the central axis, as shown in Figure 9. In the actual detection, these peak points are connected together, showing obvious linear characteristics in the image, and the wake angle can be used for pattern recognition. When the diving depth is shallow, as the velocity increases, the Froude number increases (still less than 1), and the wake angle decreases monotonously; when the diving depth is deep, the rate of the wake angle decreasing with respect of velocity (Froude number) slows down, which is consistent with the results in [14]. This phenomenon is caused by the constructive interference of the bow wave and the stern wave: According to the analysis above, as the velocity increases, the divergent wave component prevails, and the divergent wave component in the stern wave interacts with the bow wave to form a narrower wake angle. While as the diving depth increases, the divergent wave component decays rapidly, the interference between the stern divergent wave and the bow wave weakens. The wake peak point mainly appears in the transverse wave component of the bow wave, and the wake angle is basically consistent with the classical value (19.5°). The change of the wake angle does not affect the overall structure of the wake. Therefore, there is no need to worry about the impact of wake angle on the wake wavelength.

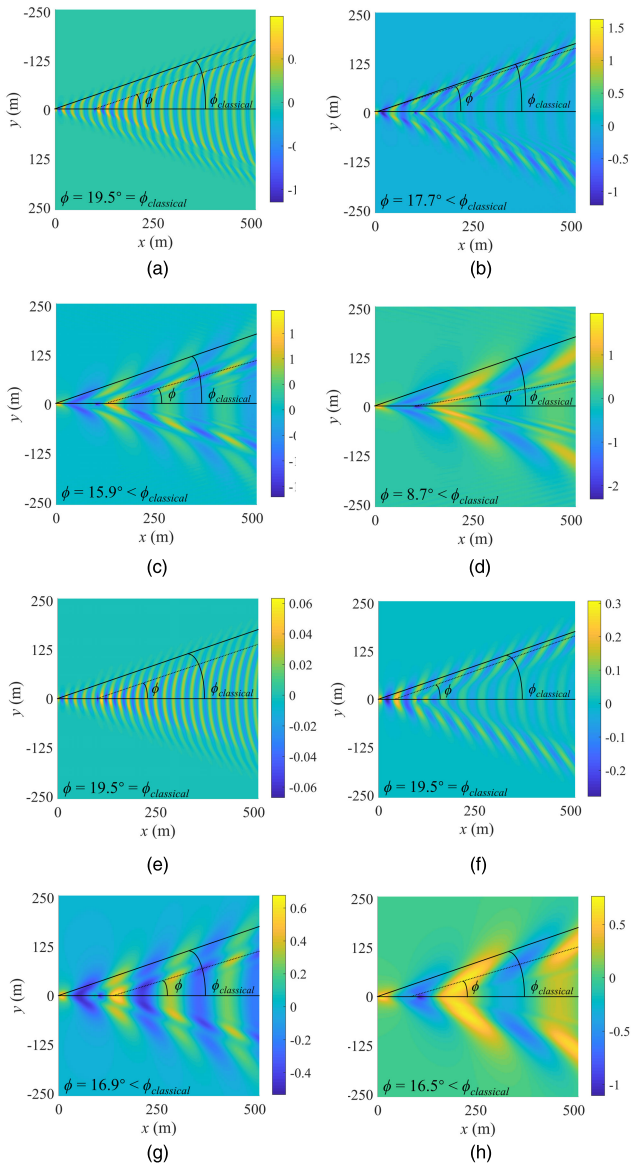

FIGURE 9. Kelvin wake angles at different velocities, U (Froude numbers, Fr_L), and diving depths, h_0. (a) $U = 6$ m/s ($Fr_L = 0.19$), $h_0 = 6$ m, (b) $U = 9$ m/s ($Fr_L = 0.29$), $h_0 = 20$ m, (c) $U = 15$ m/s ($Fr_L = 0.48$), $h_0 = 6$ m, (d) $U = 20$ m/s ($Fr_L = 0.64$), $h_0 = 6$ m, (e) $U = 6$ m/s ($Fr_L = 0.19$), $h_0 = 15$ m, (f) $U = 9$ m/s ($Fr_L = 0.29$), $h_0 = 15$ m, (g) $U = 15$ m/s ($Fr_L = 0.48$), $h_0 = 15$ m, and (h) $U = 20$ m/s ($Fr_L = 0.64$), $h_0 = 15$ m.

4) INFLUENCE OF AN APPENDAGRE

According to (19), when the speed of a submarine is constant, the shape details such as an appendage of the submarine does not affect the wake structure. We use CFD model to verify this. The appendage is an elliptic cylinder, and the length of its major and minor axes are 1/10 and 2/3 of the length and the beam of the Rankine ellipsoid. The appendage is located in the middle of the Rankine ellipsoid, and the distance from the apex of the appendage to the central axis of the ellipsoid is equal to the beam (see Figure 10). The wake wave height distribution of a submarine with/without a tower appendage at the same velocity and diving depth is shown in the Figure 11, the maximum wave height and wake angle are shown in table 1. Whether the submarine has an appendage attached or not has no effect on the Kelvin wake structure, and the wave height of the wake generated by the submarine with an appendage is slightly higher than that without an appendage. This is understandable because an

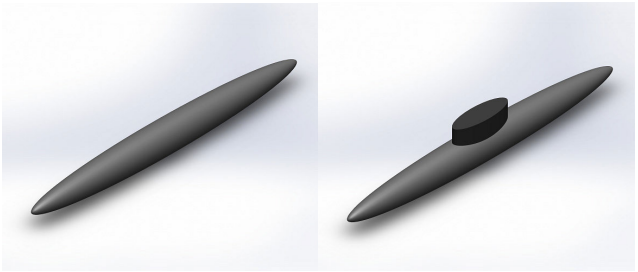

FIGURE 10. Submarine model for CFD simulation. (a) Rankine ellipsoid, submarine size, 60 m × 6 m, and (b) Rankine ellipsoid with an elliptic cylinder appendage attached, submarine size, 60 m × 6 m, appendage size, 6 m × 4 m × 6m.

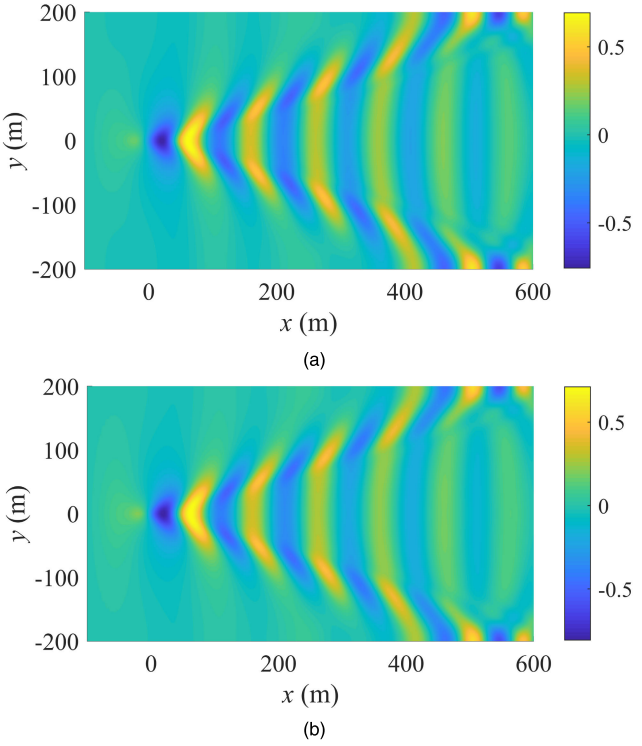

FIGURE 11. Kelvin wake patterns simulated by CFD method for a submarine with/without a tower appendage at the same velocity, $U = 12$ m/s and diving depth, $h_0 = 15$ m. (a) Rankine ellipsoid and (b) Rankine ellipsoid with an appendage attached.

TABLE 1. Kelvin wake height & wake angle under different conditions.

Diving Depth h_0 (m)	Velocity U (m/s)	Appendage attached	Maximum Wave Height (m)	Wake Angle (°)
15.00	12.00	N	0.6931	19.47°
15.00	12.00	Y	0.7118	19.47°

appendage increases the displacement of a submarine without changing the Froude number. Therefore, in the related fields of pattern recognition and photoelectric image detection, the research on the relationship between Kelvin wake and submarine parameters does not require excessive attention to the influence of submarine geometric details.

B. FOURIER POWER SPECTRUM CHARACTERISTICS OF THE KELVIN WAKES OF SUBMARINES

Although the Kelvin wake shows distinguishable divergent wave/transverse wave mode features with increasing diving depth, both components still exist at any position in the wave field, and it is difficult to separate them when they are superimposed [28]. In addition, owing to the existence of ocean waves on the sea surface, the contrast between transverse waves and divergent waves is reduced by the influence of background noise, making it difficult to separately analyze the two components from images in the space domain. However, it is feasible to analyze the wake component characteristics in the frequency domain.

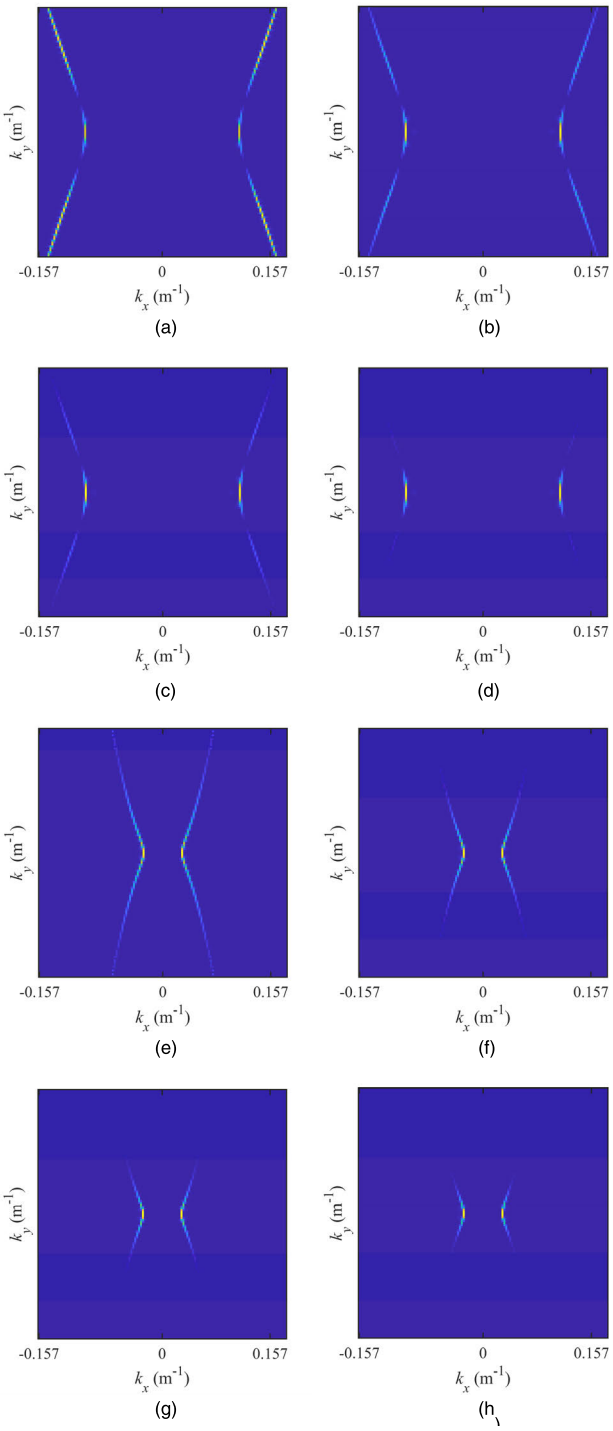

FIGURE 12. Kelvin wake Fourier power spectrum in the wavenumber space at different velocities, U, and diving depths, h_0. (a) $U = 10$ m/s, $h_0 = 10$ m, (b) $U = 10$ m/s, $h_0 = 20$ m, (c) $U = 10$ m/s, $h_0 = 30$ m, (d) $U = 10$ m/s, $h_0 = 50$ m, (e) $U = 20$ m/s, $h_0 = 10$ m, (f) $U = 20$ m/s, $h_0 = 20$ m, (g) $U = 20$ m/s, $h_0 = 30$ m, and (h) $U = 20$ m/s, $h_0 = 50$ m.

The Fourier power spectrum of a Kelvin wake wave height distribution is obtained by fast Fourier transform (FFT). The intensity distribution of the Fourier power spectrum in the wavenumber space (k_x, k_y) is shown in figure 11. The image

brightness corresponds to the power spectral intensity. The far-field Kelvin wake is seen as a distinct "X" component in the power spectrum [29], [30]:

$$k_y = \pm\frac{U^2}{g}k_x\sqrt{k_x^2 - \frac{g^2}{U^4}}$$
$$k_x = k_p\cos\theta, \quad k_y = k_p\sin\theta \tag{23}$$

At the same diving depth, as the velocity increases, the brightness of each pixel on the "X" structure increases, the energy of the power spectrum increases and the far-field "X" structure shrinks to the center. At the same velocity, as the diving depth increases, the far-field "X" structure remains unchanged, the brightness of each pixel on the "X" structure decreases and the energy decays rapidly from the outside to the inside.

As the distributions of the transverse and divergent waves on the Fourier power spectrum do not overlap (see Figure 13), the energy distribution characteristics of the two components can be discussed. For (23), when $k_y = 0$, the corresponding $k_x = \pm g/U^2$ is the cutoff wavenumber, which is reflected in two inflection points on the inner side of the "X" shape of the Fourier power spectrum. When $\theta = 35°16'$, the components of the transverse and divergent waves on the Kelvin arm are exactly separated, with $k_y/k_x = \tan 35°16' = 1/(\sqrt{2})$, and the corresponding abscissa on the Fourier power spectrum is $k_s = (\sqrt{3/2})k_0$. Transverse waves exist between k_0 and k_s, and divergent waves exist outside k_s.

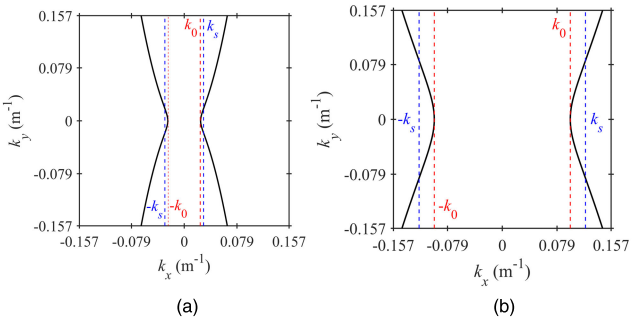

FIGURE 13. Structures of far-field Kelvin wake Fourier power spectra at different velocities, U. Solid black lines represent the "X" structure of the power spectrum in wavenumber space. The red dotted lines represent the cutoff wavenumber, k_0. The blue dotted lines represent the wavenumber where the divergent and transverse waves are exactly separated, k_s. (a) $U = 10$ m/s and (b) $U = 20$ m/s.

The Kelvin wake Fourier power spectrum image is processed by morphology to extract the transverse wave and the divergent wave, and the relationship between their energy and the motion state of a submarine is discussed. The results are given in Figure 14. The abscissa represents the diving depth, and the ordinate is the ratio of the transverse wave energy to the divergent wave energy. The results demonstrate the following: (1) As the submergence depth increases, the divergent wave attenuates faster and the variation in the energy ratio between the divergent wave and the transverse wave can be fitted by an exponential function. (2) As the speed increases,

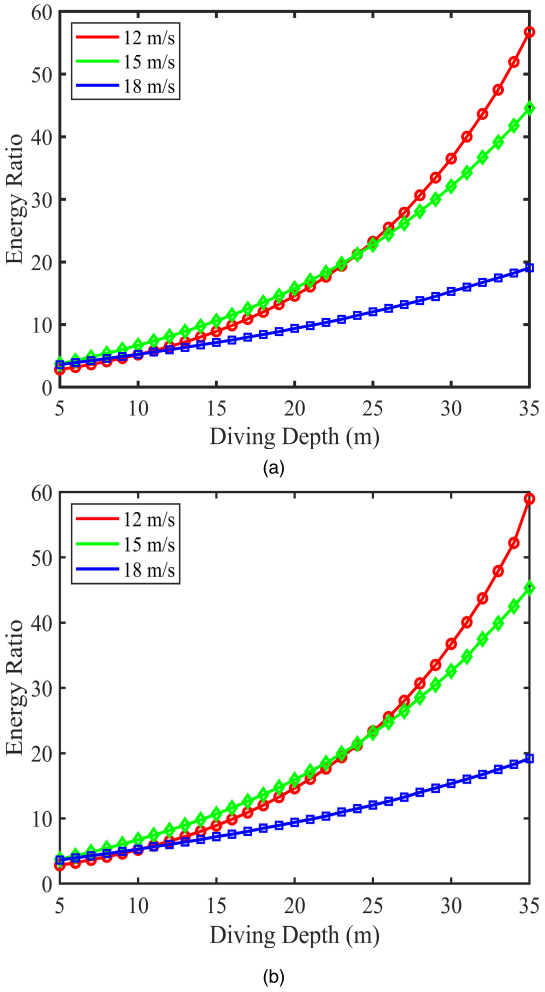

FIGURE 14. Energy ratio of Kelvin wake transverse wave components to divergent wave components under different conditions, including beam to length ratio of the submarine, velocities U, and diving depth h_0. The different velocities are drawn with lines of different colors. (a) Length to beam ratio, $l/b = 10:1$, and (b) length to beam ratio, $l/b = 7:1$.

the proportion of divergent wave energy increases and the attenuation is relatively slow. (3) For the same volume of submarines, the wake energy distribution of submarines with different length to beam ratios varies at almost the same rate as the diving depth. This indicates that as long as the volume of the submarine is determined, fine geometric structures such as appendages have little effect on the far-field wake analysis (the length to beam ratio still needs to be high to meet the thin-ship approximation criterion). The above analysis provides theoretical support for the inversion of diving depth.

C. WAVE HEIGHT DISTRIBUTION CHARACTERISTICS OF THE INTERNAL WAKE OF A SUBMARINE IN THE FAR FIELD

1) SAME DIVING DEPTH, DIFFERENT VELOCITIES

As shown in Figure 15, the trend of variation in the internal wake generated by a submarine with different velocities at the same diving depth is similar to that of a Kelvin wake,

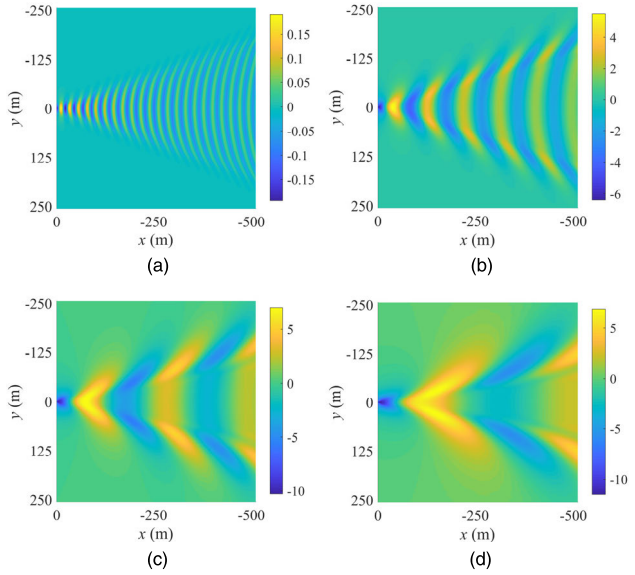

FIGURE 15. Internal wake patterns at four velocities and the same diving depth, $h_0 = 20$ m. (a) $U = 6$ m/s, (b) $U = 12$ m/s, (c) $U = 18$ m/s, and (d) $U = 24$ m/s.

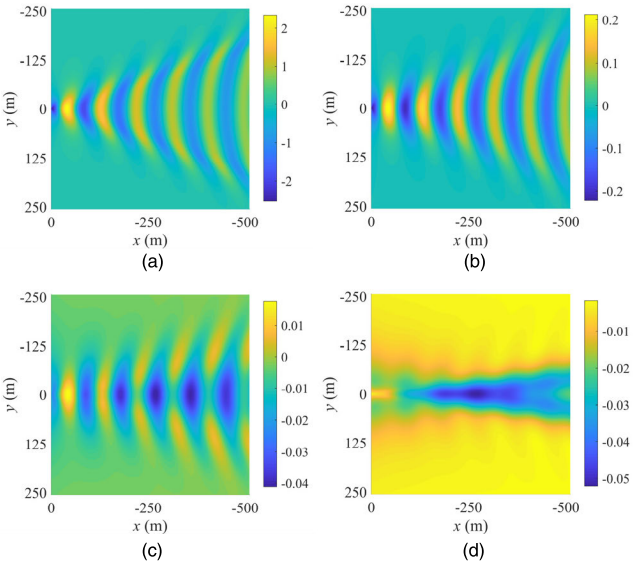

FIGURE 16. Internal wake patterns at four diving depths and the same velocity, $U = 12$ m/s. Fluid density stratified at a depth of $h_1 = 80$ m. (a) $h_0 = 30$ m, (b) $h_0 = 60$ m, (c) $h_0 = 90$ m, and (d) $h_0 = 120$ m.

and the wake wavelength (transverse wave) is equal to that of a Kelvin wake at the same submarine velocity.

2) SAME VELOCITY, DIFFERENT DIVING DEPTHS

The wave height distribution of the internal wake at different diving depths depends on stratification of the fluid. The Froude number is defined by the flow field depth, h, given by

$$Fr_h = \frac{U}{\sqrt{gh}} \tag{24}$$

Note that the Froude number in (24) is different from the Froude number based on the submerged body's length in (22). The internal wake has two critical Froude numbers [19]:

$$Fr_n^2 = \frac{1}{2} + (-1)^{n+1}\sqrt{\frac{1}{4} - \frac{(1-\gamma)h_1h_2}{h^2}}, \quad n = 1, 2 \tag{25}$$

When $Fr_h > Fr_1$, the internal wake behaves like a surface-wave mode similar to a Kelvin wake, whereas when $Fr_2 < Fr_h < Fr_1$, the internal-wave mode dominates. As shown in Figure 16, the flow field depth is 160 m, and the fluid density is stratified at 80 m depth. It can be clearly seen that as the diving depth increases, the internal wake transforms from a Kelvin surface-wave mode to a narrower internal-wave mode, and the internal wake wave height attenuation is much slower than that of the Kelvin wake. The conversion of two modes of the internal wake with increasing diving depth causes an obvious change in the wave height distribution. If there is prior knowledge of the stratification of a local ocean area, the diving depth of a submarine can be roughly estimated based on the internal wake pattern.

IV. INVERSION OF SUBMARINE MOTION INFORMATION BY A WAKE

A. VELOCITY RETRIEVAL OF A SUBMARINE

Velocity is an important part of submarine motion information and also a necessary condition for calculating the diving depth of a submarine. By accurately measuring the far-field Kelvin/internal wake wavelength, the velocity of the submarine can be directly calculated using (20) and (21). For actual detection, the following improvements are proposed:

1) When the sea condition is good and the wake structure can be clearly obtained from photoelectric detectors, using the periodicity of Fourier functions, fit the curve of the gray level of a row of pixels on the Kelvin arm and the position coordinates of the pixel points (i.e., the distance from the point along the Kelvin arm direction to the Bernoulli hump) $\zeta(x) = a_0 + a_1\cos(\omega x) + a_2\sin(\omega x)$. The Kelvin wake wavelength, $\lambda = 2\pi/\omega$, can be accurately calculated using the fitted Fourier function period, so that the velocity of the submarine can be retrieved.
2) This improvement is mainly applicable to Kelvin wakes. When the sea condition is poor, imaging devices can detect wake targets, but the periodic distribution of the wake is blurred. First use median filters to remove wave noise from the wake image; then use FFT to extract the "X" structure of the wake Fourier power spectrum. The motion velocity of a submarine can be calculated from the deformation of (23) as follows:

$$U = \sqrt{\frac{gk_y}{k_x\sqrt{k_x^2 - \frac{g^2}{U^4}}}} \tag{26}$$

CFD simulated images (flow field size, 700 m × 400 m; resolution, 0.5 m; submarine size, 60 m × 6 m, without appendages) of Kelvin wakes induced by a submarine at a speed of 13.00 m/s and a diving depth of 15 m are taken as measured data to verify the accuracy of velocity retrieval of the above method. The direct inversion velocity is 13.61 m/s with an error of 4.69%. The improved method 1 has a retrieval velocity of 13.49 m/s with an error of 3.77%. The improved method 2 has a retrieval velocity of 13.24 m/s with an error of 1.85%. Because the Kelvin wake has a relatively stable structure, the accuracy of the improved method 2 is relatively high. The computational complexities of the above algorithms differ; appropriate methods can be selected according to actual requirements.

B. KELVIN WAKE INVERSION OF DIVING DEPTH

The diving depth of a submarine does not affect the Kelvin wake structure. However, it affects the wake wave height/energy characteristics. Currently, the diving depth of a submarine can only be analyzed using the Kelvin wake from the wave height/energy distribution. According to the thin-ship approximation, the Fourier power spectrum integral of the far-field Kelvin wake can be regarded as a set of products of the square of the Kochin function, F (representing hull shape), at each frequency point of the "X" structure and the exponential attenuation term. The relationship between the Fourier power spectrum intensity, $S(k)$, and the abscissa, k_x, is given by $S(k_x) = \exp(-2\,hk_x/k_0)\cdot F^2(k_x)$. By analyzing the waveform of the square of the Kochin function of the Rankine ellipsoid, the function can be approximately expressed as an oscillation function multiplied by an exponential function:

$$F^2(k_x) = F_2(k_x)\exp(fk_x) \tag{27}$$

where $F_2(k_x)$ is the oscillating part of the square of the Kochin function. The intensity of the far-field Kelvin wake Fourier power spectrum can be expressed as

$$\begin{aligned} S(k_x) &= F_2(k_x)\exp(fk_x)\exp(-\frac{2hk_x}{k_0}) \\ &= F_2(k_x)\exp[-\frac{2(h+A)k_x}{k_0}] \end{aligned} \tag{28}$$

where A refers to the influence of the Kochin function on the curvature of the exponential function. For a certain range of the diving depth, the exponential function plays a decisive role in the intensity distribution of the entire power spectrum whereas the oscillation function plays a modulation role. The Fourier power spectrum intensity can be fitted as a function of the abscissa, k_x, by an exponential function. On the basis of the above discussion, we propose the following simple method for submarine diving depth inversion:

1) This method needs prior information regarding the size of the target to be detected. The size of current mainstream submarines is about 100 m × 10 m.
2) Remove the background noise due to ocean waves and retrieve the target speed using the above methods.
3) Use potential flow theory to calculate the Fourier power spectra of n (n ≥ 1) Kelvin wakes generated by a Rankine ellipsoid of a similar size as the target at a speed U and at different diving depths h_i. For each image of the power spectrum, extract the transverse wave component (decays slower with diving depth) by morphology and obtain the transverse wave power spectral intensity row vector by summing the columns of the image. Fit all these row vectors with an exponential function (28) to obtain n $h_i + A_i$. Because h_i is the input parameter of the potential flow method, n A_i can be obtained.
4) The "X" shape distribution of the Fourier power spectra of wakes induced by submarines with the same speed and different diving depths does not change, and the Kochin function at the same spectrum position does not change with diving depth; therefore, the n A_i are approximately equal. The average value A of Ai can be regarded as the effect of the Kochin function of the target on the curvature of the exponential function under real conditions.
5) Obtain the Fourier power spectrum of the wake to be detected. The fitting method in step 3) is used to obtain $h_{measure} + A$. Finally, subtract A to obtain the measured diving depth $h_{measure}$.

CFD simulated images are still used as actual detection data to verify the accuracy of the algorithm (flow field size, 700 m × 400 m; resolution, 0.5 m; submarine size, 60 m × 6 m, with or without appendages). The results are shown in Table 2. The maximum inversion error of the diving depth is less than 6.8%, which indicates the accuracy of the method for a given diving depth range. The attachment of a submarine command tower has little effect on the inversion accuracy of velocity and diving depth, which is consistent with the analysis in Section III.B. The results show that the method has practical application prospects.

TABLE 2. Velocity and diving depth inversion for the proposed method.

Actual values (ANSYS Fluent)			Calculated values		
Velocity U (m/s)	Diving depth h (m)	Appendage attached	Output A	Velocity U (m/s)	Diving depth h (m)
20.00	15.00	N	−3.46	20.32	15.87
20.00	15.00	Y	−3.46	20.31	15.73
15.00	15.00	N	4.57	15.35	16.02
15.00	15.00	Y	4.59	15.21	15.95

The method is further discussed as follows: 1) It does not directly measure the energy of the Kelvin wake. 2) Regular noise, such as background ocean waves, has little effect on the inversion accuracy. 3) When the length to beam ratio of a submarine is constant, the shape details such as an appendage have little effect on the inversion accuracy. 4) We drew curves of variation of the output parameter, $(h_i + A_i)$, in the potential flow theory model with the input diving depth at different velocities (Rankine ellipsoid size, 60 m × 6 m; see Figure 17 for the curve), and discussed the achievable

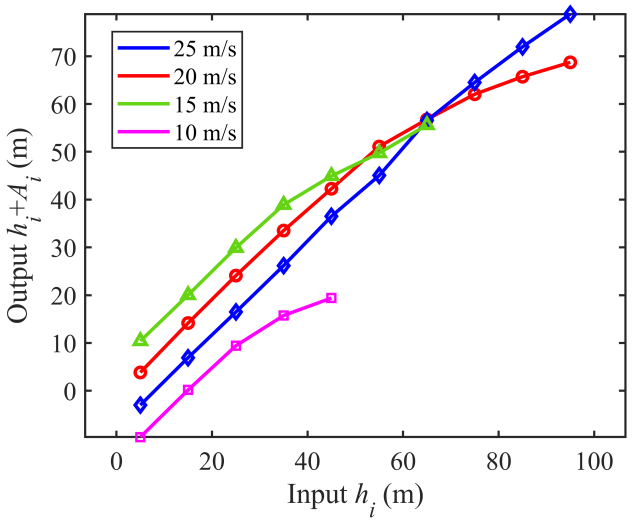

FIGURE 17. Relationship between the output parameter ($h_i + A_i$) and the input depth h_i at different velocities in the potential flow theory model. The different velocities are drawn with lines of different colors.

theoretical inversion range of the method. It can be seen that the maximum detection range increases with increasing velocity. When the diving depth is shallow, the curve indicates a straight line with a slope of 1, which shows that the method can accurately invert the diving depth. When the diving depth exceeds a certain range, the slope of the curve begins to change at different velocities because of the larger h_i, the rapid attenuation of $\exp[-2(h_i + A)k_x/k_0]$, and the gradual nonnegligible effect of $F_2(k_x)$. The occurrence of the inflection point of the slope variation lags as the increase in velocity. The theoretical range for diving depth inversion can reach 100 m at 25 m/s velocity (the maximum speed known to be achieved by existing submarines). It is worth noting that the initial value of the curve at 10 m/s is inconsistent with its initial value at other velocities. This is because the transverse component of the Kelvin wake Fourier spectrum at 10 m/s is located at the "rising edge" of $F_2(k_x)$ oscillation, whereas the other cases are located at its "falling edge". 5) It is more likely to generate detectable internal wakes when a submarine moves undersea deeper than 100 m. Similar analysis of the surface-wave mode of internal wakes can be considered for the submarine diving depth inversion.

V. CONCLUSION

The study of the relationship between the characteristics of water surface wakes and the velocity and diving depth of an underwater moving target is a key link in submarine wake detection. In this paper, the Kelvin wake and the internal wake are modeled by the potential flow theory method, and the characteristics of the wake are quantitatively analyzed. On the basis of the Fourier power spectrum characteristics of Kelvin wakes, we proposed a method for submarine diving depth inversion. The simulation results show that the proposed method has a theoretical achievable maximum measurement range of 100 m, with an error of less than 10% at a diving depth of 50 m. Kelvin wakes below 100 m are difficult to detect; therefore, other methods can be considered. Utilizing the water surface ripple pattern induced by underwater moving targets for submarine detection and identification is a promising method. It is of great practical value for exploring effective imaging and analysis methods for surface ripples.

REFERENCES

[1] G. Zilman, A. Zapolski, and M. Marom, "The speed and beam of a ship from its wake's SAR images," *IEEE Trans. Geosci. Remote Sens.*, vol. 42, no. 10, pp. 2335–2343, Oct. 2004.

[2] G. Zilman, A. Zapolski, and M. Marom, "On detectability of a sKelvin wake in simulated SAR images of rough sea surface," *IEEE Trans. Geosci. Remote Sens.*, vol. 53, no. 2, pp. 609–619, Feb. 2015.

[3] J. Tunaley, E. Buller, K. Wu, and M. Rey, "The simulation of the SAR image of a ship wake," *IEEE Trans. Geosci. Remote Sens.*, vol. 29, no. 1, pp. 149–156, Jan. 1991.

[4] K. Oumansour, Y. Wang, and J. Saillard, "Multifrequency SAR observation of a ship wake," *IEEE Proc.-Radar, Sonar Navigat.*, vol. 143, no. 4, pp. 275–280, Aug. 1996.

[5] M. Zhang and J. Li, "Numerical simulation and analyses of SAR images from ship wakes," in *Proc. Int. Appl. Comput. Electromagn. Soc. Symp. (ACES)*, Miami, FL, USA, 2019, pp. 1–2.

[6] S. Zhang, Z. Yang, and L. Yang, "Multi-directional infrared imaging characterization of ship Kelvin wake," in *Proc. Int. Conf. Ind. Control Electron. Eng.*, Xi'an, China, 2012, pp. 144–146.

[7] X. Chen, C. Lin, and L. Yang, "Simulation of infrared characterizations and detection of Kelvin wake," *Infr. Technol.*, vol. 39, no. 8, pp. 717–721, Aug. 2017.

[8] V. Issa and Z. A. Daya, "Modeling the ship white water wake in the midwave infrared," *Appl. Opt.*, vol. 57, no. 35, pp. 10125–10134, 2018.

[9] Z. Xu, C. Du, and M. Xia, "Evaluation of electromagnetic fields induced by wake of an undersea-moving slender body," *IEEE Access*, vol. 6, pp. 2943–2951, 2018.

[10] Z. Xu, C. Du, and M. Xia, "Electromagnetic fields due to the wake of a moving slender body in a finite-depth ocean with density stratification," *Sci. Rep.*, vol. 8, no. 1, pp. 2943–2951, 2018.

[11] J. T. Morris and S. J. Anderson, "Statistical polarimetric radar detection of submerged obstacles via perturbed flows on the ocean surface," in *Proc. Int. Conf. Electromagn. Adv. Appl.*, Sydney, NSW, Australia, 2010, pp. 275–278.

[12] S. Ellingsen, "Ship waves in the presence of uniform vorticity," *J. Fluid Mech.*, vol. 742, p. R2, Jan. 2014.

[13] H. Wu, J. He, H. Liang, and F. Noblesse, "Influence of Froude number and submergence depth on wave patterns," *Eur. J. Mech.-BFluids*, vol. 75, pp. 258–270, May 2019.

[14] M. M. Amiri, S. H. Sphaier, M. A. Vitola, and P. T. Esperança, "Investigation into the wave system of a generic submarine moving along a straight path beneath the free surface," *Eur. J. Mech. B-Fluid.*, vol. 76, pp. 98–114, Jul. 2019.

[15] J. M. Kuo and K.-S. Chen, "The application of wavelets correlator for ship wake detection in SAR images," *IEEE Trans. Geosci. Remote Sens.*, vol. 41, no. 6, pp. 1506–1511, Jun. 2003.

[16] F. Biondi, "A polarimetric extension of low-rank plus sparse decomposition and radon transform for ship wake detection in synthetic aperture radar images," *IEEE Geosci. Remote Sens. Lett.*, vol. 16, no. 1, pp. 75–79, Jan. 2019.

[17] J. Fitch, S. Lehman, F. Dowla, S. Lu, E. Johansson, and D. Goodman, "Ship wake-detection procedure using conjugate gradient trained artificial neural networks," *IEEE Trans. Geosci. Remote Sens.*, vol. 29, no. 5, pp. 718–726, Sep. 1991.

[18] A. Arnold-Bos, A. Martin, and A. Khenchaf, "Obtaining a ship's speed and direction from its Kelvin wake spectrum using stochastic matched filtering," in *Proc. IEEE Int. Geosci. Remote Sens. Symp.*, Barcelona, Spain, Jul. 2007, pp. 1106–1109.

[19] F. Liang and Y. Chen, "A ship velocity inversion method of ship Kelvin wakes in SAR images," *Sci. Tech. Eng.*, vol. 11, no. 20, pp. 4793–4799, Jul. 2011.

[20] T. Gourlay and E. Dawson, "A Havelock source panel method for near-surface submarines," *J. Mar. Sci. Appl.*, vol. 14, no. 3, pp. 215–224, 2015.

[21] J. Newman, *Marine Hydrodynamics*. Cambridge, MA, USA: MIT Press, 1977.
[22] D. Scullen and E. O. Tuck, "Nonlinear free-surface flow computations for submerged cylinders," *J. Ship Res.*, vol. 39, no. 3, pp. 185–193, 1995.
[23] D. Li, W. Jin, L. Li, X. Lu, and S. Qiu, "Numerical simulation and analysis of free-surface wake generated by moving submerged target," *Infr. Laser Eng.*, vol. 47, no. 11, pp. 456–463, Nov. 2018.
[24] E. O. Tuck and D. Scullen, "A comparison of linear and nonlinear computations of waves made by slender submerged bodies," *J. Eng. Math.*, vol. 42, nos. 3–4, pp. 255–264, 2002.
[25] R. W. Yeung and T. C. Nguyen, "Waves generated by a moving source in a two-layer ocean of finite depth," *J. Eng. Math.*, vol. 35, nos. 1–2, pp. 85–107, 1999.
[26] G. Wei, D. Lu, and S. Dai, "Waves induced by a submerged moving dipole in a two-layer fluid of finite depth," *Acta Mechanica Sinica*, vol. 21, no. 1, pp. 24–31, 2005.
[27] A. Wang and M. Zhu, "Fast simulation of ocean features imaging by SAR," *High Technol. Lett.*, vol. 12, no. 10, pp. 79–84, 2002.
[28] Y.-X. Sun, P. Liu, and Y.-Q. Jin, "Ship wake components: Isolation, reconstruction, and characteristics analysis in spectral, spatial, and TerraSAR-X image domains," *IEEE Trans. Geosci. Remote Sens.*, vol. 56, no. 7, pp. 4209–4224, Jul. 2018.
[29] W.-Y. Zhang, D.-H. Hu, and C.-B. Ding, "Enhancement of SAR ship wake image based on FABEMD and Goldstein filter," *J. Radars*, vol. 1, no. 4, pp. 426–435, May 2013.
[30] G. Gomit, G. Rousseaux, L. Chatellier, D. Calluaud, and L. David, "Spectral analysis of ship waves in deep water from accurate measurements of the free surface elevation by optical methods," *Phys. Fluids*, vol. 26, no. 12, 2014, Art. no. 122101.

FUDUO XUE received the B.S. degree in optoelectronic information engineering from Beijing Jiao Tong University, Beijing, China, in 2018. He is currently pursuing the Ph.D. degree with the School of Optoelectronics, Beijing Institute of Technology, Beijing. His research interests are photoelectric imaging detection techniques and instruments, especially for polarization imaging theories and devices for water surface wake detection.

WEIQI JIN received the Ph.D. degree in military optics from the Beijing Institute of Technology, China, in 1990. He has been the Ph.D. Tutor, a Professor, and the Director of the Key Laboratory of Opto-Electronic Imaging Technology and Systems, Beijing Institute of Technology. He is currently the Director of the Chinese Optical Society and the Beijing Institute of Optics, and an Advanced Member of the Chinese Institute of Electronics. His main research interests include polarization imaging technology, photoelectric image processing, and photoelectric detection and instrumentation.

SU QIU received the B.S. and Ph.D. degrees in optical engineering from the Beijing Institute of Technology, Beijing, China, in 2003 and 2013, respectively. He has been the Master's Supervisor and a Lecturer with the Key Laboratory of Opto-Electronic Imaging Technology and Systems, Beijing Institute of Technology. His main research interests include image information processing, photoelectric detection, and photoelectric imaging technology.

JIE YANG received the B.S. degree in optical information and technology from the Beijing Institute of Technology, Beijing, China, in 2017, where she is currently pursuing the Ph.D. degree with the School of Optoelectronics. Her research interests are polarization imaging technology and its application, including the application of polarization imaging in the water surface wakes detection and restoration.